A Consensus-based Distributed Temperature Priority Control of Air Conditioner Clusters for Voltage Regulation in Distribution Networks

Zhuang Zheng, *member, IEEE*, Shengwei Wang, Wenzhuo Li, Xiaowei Luo

***Abstract*—High penetration of Photovoltaic (PV) to the distribution network may bring under-voltage and over-voltage issues, limiting the PV hosting capacity. Air conditioners (AC) in grid-interactive buildings can support voltage regulation by manipulating flexible energy consumption. This paper developed a novel voltage control strategy to regulate the AC clusters' on/off states for distribution network voltage regulation under high PV penetrations. The novelty lies in the distributed formulation of temperature priority-based on/off control (TPC) of AC clusters and the strategic selection and permutation of demand response technologies, including the real-time optimal demand response resources dispatch, distributed sensing of ACs based on average consensus algorithm, and the local implementation of TPC strategy and trial calculation scheme for flexibility capacity estimation. Finally, the distributed TPC is validated to be effective for system rebalancing with no comfort violations and an acceptable ON/OFF switching frequency. The theoretical and numerical analysis also proves its scalability and robustness to communication delays and link failures. It is then incorporated into a novel hierarchical control framework for smart grid voltage control in a four-bus three-phase test grid, considering the voltage sensitivities to power injections in different locations and phases.**

***Index Terms*—average consensus, distributed, temperature priority control, hierarchical voltage control, air conditioners, distribution network.**

I. Introduction

THE growing use of rooftop PVs connected to the low voltage distribution networks (LVDN) may induce technical issues [1], [2]. One of the main challenges is the voltage rise/drop problems due to the mismatch between variable PV generations and local demands. Various solutions have been proposed for voltage regulation of distribution networks. The simplest way is grid reinforcement, such as installing shunt capacitors, on-load tap changing (OLTC) transformers, and voltage regulators, which is effective but expensive. Furthermore, they were initially designed for the traditional grid without an extensive penetration of distributed generators (DGs). With the increasing of low-inertia DGs like PV panels, the voltage regulators and OLTCs may face time delay issues. The shunt capacitor bank may induce excessive line losses due to the increased flowing reactive powers.

Though reactive power management [3] is often used for transmission network voltage regulation, the active power management has gained growing popularity in distribution network voltage regulation due to the high ratios of line resistance to reactance (R$\gg$X) [4], [5]. In this context, demand response (DR) is a promising way to regulate grid voltage by manipulating flexible energy consumptions, especially the building air conditioners (ACs). Seng and Taylor [6] validated the effectiveness of DR for mitigating voltage rise problems by simulating a distribution network and two wind turbines. Xie et al. [7] found that using the elastic demand for voltage regulation can reduce the operation times of OLTC transformers. Elizabeth et al. [8] proposed distributed and adaptive receding horizon optimization-based approaches to manage the supply voltages and power flows in a distribution grid with residential PV-battery systems. Jiang et al. [9] proposed a smoothing control of ACs to mitigate the net demand fluctuations induced by volatile PV generations and eliminate the tap operations of voltage regulators. Chandran et al. [10] presented a coordinated load curtailment method for voltage regulation in LVDN. Dong [11] also indicated that the building thermal load could reduce voltage drops by predictive controls.

Different control strategies of ACs for voltage regulation can be divided into local, centralized, and distributed methods. Local control strategies calculate control actions only using locally measured information, such as the droop control and on/off thermostat control. Because it is cheap and easy to implement, the local control strategies are the most practical methods for voltage control. Klem et al. [12] demonstrated how the droop control of flexible loads and the generation could stabilize the system effectively. Though fast and naïve, they are criticized for the short-sight and sub-optimal solutions in long-term energy management. For example, the predictive local PV outputs and demands can be leveraged for proactive voltage management. The heterogeneous and dispersed distributed generators and voltage control measures should be coordinated to produce cooperative actions.

The centralized methods calculate control actions with all the relevant information about the networks and components and send back individual control commends through a star communication network. The most common centralized methods in the literature are the optimization-centric methods. Fontenot et al. [11] proposed a centralized model predictive control for coordinated voltage regulation and energy man-

Zhuang Zheng and Shengwei Wang are with the Department of Building Environment and Energy Engineering, The Hong Kong Polytechnic University, Hung Hom, Hong Kong

Wenzhuo Li is with The Bartlett School of Environment, Energy and Resources, University College London, London, UK

Xiaowei Luo *(Corresponding author, email: xiaowluo@cityu.edu.hk)* is with the Department of Architecture and Civil Engineering, City University of Hong Kong, Kowloon Tong, Hong Kong

agement by integrating buildings, PV inverters, and batteries into the power distribution network and jointly optimizing all components. Jiang et al. [13] also developed an integrated building-to-grid (B2G) optimization model to reduce the grid loss and increase the voltage magnitude by the flexible operation of ACs. Though the optimization-centric methods are optimal, they may be impractical due to the high computation and communication burden and high data requirement.

Alternatively, the temperature priority control (TPC) of AC clusters is a rule-based centralized control strategy with lower complexity. The central coordinator of TPC collects the state information of each AC in the network and selects ACs to be turned on/off based on the requested DR amount and the ON/OFF priority lists generated by the difference between indoor temperatures and setpoints. Lu et al. [14] applied TPC to control thermal loads for continuous regulation reserves. Wu [15] adopted the TPC of AC clusters for fast primary frequency regulation. Hu et al. [16] extended the TPC by incorporating a novel swapping mechanism and the up/down reserve bounds to improve thermal comfort and guarantee tacking capability. The modified TPC was further used in the AC systems of commercial buildings for peak load reduction and load shaping [17]. However, the above TPCs all require central coordinators to collect the state information of each AC and send the individual controls, which is impractical due to the high communication cost and privacy concerns.

Recently, consensus-based distributed controls, relying on no central coordinator but only sparse communication links among neighboring agents, have gained popularity for the fair task/resource allocation of voltage or energy management [18]–[20]. Zeraati et al. [5] combined the local voltage droop control and the consensus control of batteries for fast and fair utilization of storage flexibility in LVDN voltage control under high PV penetrations. They further applied the consensus algorithms to other applications in distribution networks, such as the cooperative voltage control of electric vehicle battery and PV active power curtailment [21] and voltage quality improvement using reactive power capability of PV inverters [22]. The above works focused on the fair allocation of voltage control efforts but neglected the efficiency of task allocations. For example, different buses and phases have different voltage sensitivities to power variations. The electric battery is also less economic and environmental-friendly than the inherent thermal storage of buildings. Zhang et al. [23] proposed a consensus control strategy of inverter AC clusters to share the adjusted temperature interval ratios for renewable energy integration. Chen et al. [24] utilized the average consensus algorithm to allocate the portions of the desired aggregated demand profile to each building energy controller in a distributed way. Since the control variables of both Zhang and Chen's methods are continuous ratio values, the control performance is sensitive to stochastic communication delays due to the deviated consensus values of consensus algorithms [25].

Although the hierarchical control of AC clusters for smart grid has been widely explored, they have some limitations. For example, Wu et al. [15] proposed a hierarchical control for primary frequency regulation using residential HVAC loads, consisting of a load aggregator, a central controller, and a group of local controllers. Nevertheless, the coordination among multiple HVAC units in a single group relied on an expensive and unscalable star communication network. The central controller dispatches the multiple HVAC loads by sending the triggering frequency to each HVAC unit. The local controller determines the ON/OFF status of HVAC units autonomously based on the triggering frequencies. It is also challenging to determine the trigger frequency setting. Wang et al. [26] adopted a two-level consensus-driven distributed control strategy to share the required active power adjustment among ACs for voltage regulation and overloading management. A star communication network among the aggregator and its group members is also needed, which is not scalable and practical. The lower-level AC units are responsible for sending maximum controllable power and receiving ON/OFF control commands to/from the upper-level aggregator. Only a few AC aggregators are coordinated through distributed consensus algorithms, ignoring the scalability to large network sizes.

Zeraati et al. [5] proposed a two-layer consensus-driven distributed control of batteries for distribution network voltage regulation under high PV penetration. The upper level uses a local droop control to determine the required power changes at each bus. Then, the battery chargers in the lower level are coordinated through consensus algorithms to make further adjustments based on their capacities and dynamics. However, the local droop controller neglected the location-dependent and phase-coupled effects of load variations on voltage profile. A few batteries are coordinated through consensus algorithms while ignoring the scalability to large network sizes.

Aiming at these shortcomings, this paper proposes a novel and practical tri-level hierarchical control framework of AC clusters for smart grid voltage control. The novelty lies in the distributed formulation of temperature priority-based on/off control (TPC) of AC clusters and the strategic selection and permutation of demand response technologies, including the real-time optimal DR resources dispatch among a few aggregators for multi-bus and multi-phase voltage regulation, distributed states sensing of multiple ACs and the local temperature priority-based on/off control and trial calculation scheme for flexibility capacity estimation. Compared to prior studies, the major contributions are listed as follows:

1) A distributed temperature priority-based control (TPC) method of AC clusters is developed for the first time to provide continuous regulation reserves for the smart grid. The local TPC controller makes on/off decisions based on the local priority lists of each AC generated by the average consensus algorithm with *Mean Metropolis* weights. Novel trial calculation schemes of ACs are proposed to derive bounds for the regulation signal within which the users' thermal comfort is guaranteed.
2) We proved that the distributed TPC scheme with *Mean Metropolis* weights is stable under time-varying communication graphs with stochastic link failures and is insensitive to the communication delays due to the binary control output. The scalability to thousands of ACs is also validated for high connectivity communication graphs, such as rectangular and cubic grids.

3) A novel and practical hierarchical control framework is proposed for efficient and effective smart grid voltage regulation through strategic selection and permutation of demand response technologies. It captures the location-dependent and phase-coupled effects of load variations on voltage profile and produces optimal solutions with limited computational burden due to the existence of AC aggregators. The proposed distributed TPC method is also superior to centralized TPC-based methods due to the robustness to communication delays and link failures and the scalability to large network sizes. The local TPC controller has straightforward functions and operates in real-time discrete intervals, which is fast and easy to implement.

II. PROBLEM DESCRIPTION

A. Voltage regulation with high penetration of PV sources

The impact of PV sources on distribution network voltage can be analyzed by the equivalent circuits in Fig. 1. First, consider the single phase network in Fig. 1a. It can be proved [5] that the voltage magnitude at the point of common coupling (PCC) can be approximated as

$$|V_n| = |V_g| + \frac{R \cdot P + X \cdot Q}{|V_g|} \tag{1}$$

where $|V_g|$ is the voltage magnitude at the source node, R and X are the line resistance and reactance, P and Q are the total active and reactive powers produced by PV and load (negative source), P=P_{pv}-P_L,Q=Q_{pv}-Q_L. Equation (1) indicates that if P is positive ($P_{pv} > P_L$), the PCC voltage increases and conversely, if P is negative ($P_{pv} < P_L$), $|V_n|$ decreases.

When PVs are unevenly installed, the three-phase distribution system may become unbalanced, and there is current flowing through the neutral conductor in the residential four-wire network, as shown in Fig. 1b. This current flow causes voltage drop over the neutral conductor and shifts the neutral voltages at all PCCs. As a result, active power changes in one phase can affect the voltages of the two other phases. Therefore, voltage regulation in the distribution network is challenging.

B. Thermodynamic and Electrical Modeling of AC

This study leverages the thermal flexibility of buildings for voltage regulation by regulating the ACs' power consumption. The thermodynamic and electrical models of buildings and ACs are described as follows. The equivalent thermal parameter (ETP) model in [27] described by (2) is a common model to approximate the thermal dynamics of a simplified AC system.

$$\begin{aligned} \dot{T}_a^t &= \tfrac{1}{C_a}(U_a[T_o^t - T_a^t] + U_m[T_m^t - T_a^t] + Q_a^t) \\ \dot{T}_m^t &= \tfrac{1}{C_m}(U_m[T_a^t - T_m^t] + Q_m^t) \end{aligned} \tag{2}$$

where the wall and indoor air temperatures (T_m,T_a) are functions of internal and external heat transfers, such as internal heat gains (Q_i), solar gains (Q_s) and heat injected/removed by ACs (Q_{AC}) (3), where f_{AC}, f_s, and f_i are fractional coefficients.

$$\begin{aligned} Q_a^t &= (1 - f_{AC})Q_{AC}^t + (1 - f_s)Q_s^t + (1 - f_i)Q_i^t \\ Q_m^t &= f_{AC}Q_{AC}^t + f_sQ_s^t + f_iQ_i^t \end{aligned} \tag{3}$$

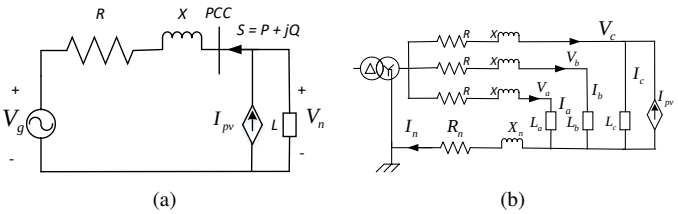

Fig. 1: Equivalent circuits of (a) a single-phase network with PV sources and (b) uneven PV installations on three-phase systems.

As for the electrical model of the AC system, the relationships among AC electrical power (P_{AC}), the cooling capacity of AC (Q_{AC}), and the ON/OFF states of the compressor (u_{AC}) can be expressed as (4), where μ_{AC} is the Coefficient of Performance for the AC system. Assuming the ACs work at cooling mode in this study, there is a minus sign before the symbols.

$$Q_{AC}^t = -\mu_{AC}^t P_{AC}^t u_{AC}^t, u_{AC}^t \in \{0, 1\} \tag{4}$$

III. PROPOSED VOLTAGE CONTROL SCHEME

Fig. 2 shows the overall diagram of the proposed control method of AC clusters for distribution network voltage regulation. The proposed method integrates central real-time optimal DR resources dispatch, distributed sensing of AC states based on average consensus algorithm, and local temperature priority-based ON/OFF control, each used for specific objectives.

We consider the three-phase four-wire electricity grid with multiple buses, each bus populated with AC-equipped grid-responsive houses and distributed PV sources. In case the voltage of a particular bus deviates from the pre-defined limits, the central real-time optimal controller in the first level determines the optimal DR amount at each phase of each bus. The required DR amounts are then sent to the aggregators for the second-level control. In the second level, the ACs of each aggregator share their state information through sparse communication links. The priority lists are locally generated for each AC by a distributed information discovery process based on the average consensus algorithm. In the third level, the local TPC controller decides its ON/OFF actions based on the required DR amount and the local priority list, similar to the centralized TPC.

A. Central Real-Time Optimal Dispatch of DR Resources

First, a voltage sensitivity-based linear programming model is developed to determine the real-time optimal DR resources dispatch among AC aggregators of different buses and phases, considering their different voltage sensitivities to the power injections. The optimal DR amount for each AC aggregator is obtained by solving the linear programming problem in (5) at each timestep t when DR is activated. The objective function includes the DR costs and the penalty of voltage deviations ($\boldsymbol{\epsilon}$) to the required voltage regulation amount ($\Delta\mathbf{U}$).

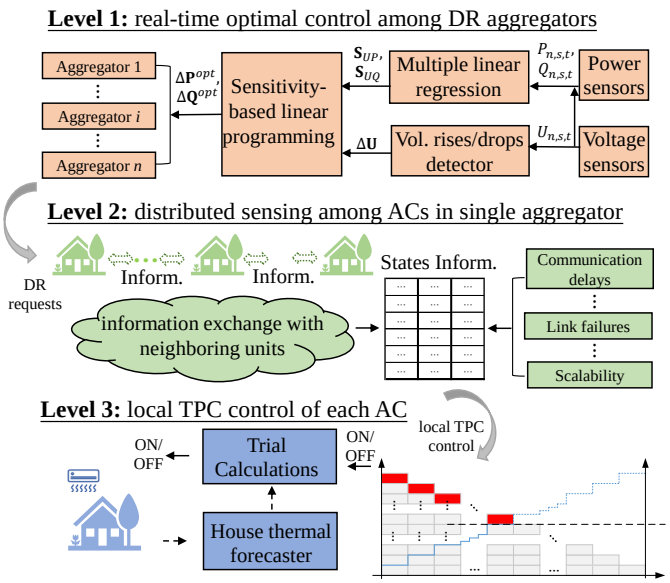

Fig. 2: Tri-level control framework for distribution network voltage regulation.

The optimized control variables are the required DR active and reactive powers $\Delta\mathbf{P}/\Delta\mathbf{Q}$.

$$\begin{aligned} &\min\left[\mathbf{\Delta P},\mathbf{\Delta Q}\right]\mathbf{W}\left[\mathbf{\Delta P},\mathbf{\Delta Q}\right]^T+\varepsilon^T\mathbf{R}\varepsilon \\ &\Delta\mathbf{U}=\left[\mathbf{S}_{UP},\mathbf{S}_{UQ}\right]\cdot\left[\mathbf{\Delta P},\mathbf{\Delta Q}\right]^T+\varepsilon \\ &\mathbf{\Delta P}\in[\mathbf{\Delta P}_{\min},\mathbf{\Delta P}_{\max}],\mathbf{\Delta Q}\in[\mathbf{\Delta Q}_{\min},\mathbf{\Delta Q}_{\max}] \\ &\mathbf{\Delta Q}=\mathbf{\Delta P}*\tan(\operatorname{acos}(PF_{AC})) \end{aligned} \tag{5}$$

where $\mathbf{S_{UP}}$ and $\mathbf{S_{UP}}$ are voltage sensitivity matrices that can be estimated from historical measurement data using methods like multiple linear regression [28], $\boldsymbol{\epsilon}$ is the slack vector to avoid problem infeasibility, $\mathbf{R}$ and $\mathbf{W}$ are the weighting matrices for trading off between the voltage control performance and the DR cost. Since the AC units consume both active and reactive powers, we relate the DR reactive power support with the active power by constant power factors of AC units PF_{AC}.

B. Distributed sensing of ACs

This subsection develops a distributed TPC method based on the average consensus algorithm for DR implementation within single aggregators. The key idea is to let each AC obtain temperature priority lists of all ACs in the network through iterative information exchanges among its neighbors. Then each AC determines its switching actions according to a common rule the same as the centralized TPC, as illustrated in Fig. 3. It is essentially a distributed information discovery process based on average consensus algorithms.

According to the average consensus algorithm, every agent can obtain the global network information through iterative information exchanges with neighbor agents in a multi-agent network. The information exchange law is defined as

$$x_i[k+1]=x_i[k]+\sum_{j\in N_i}a_{ij}(x_j[k]-x_i[k]) \tag{6}$$

where $i,j\in\{1,\ldots,r\}$ are the indices of r AC units, $x_i[k]$ and $x_i[k+1]$ are the discovered information by the agent i at the

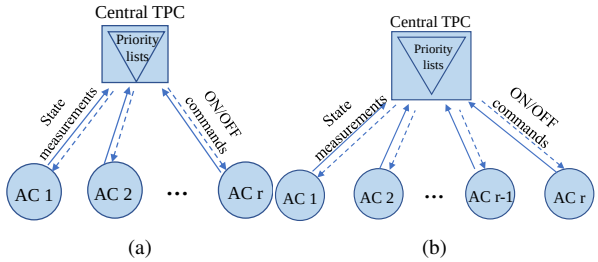

Fig. 3: Diagrams of (a) centralized TPC, (b) distributed TPC.

k and $k+1$ iteration, respectively. a_{ij} is the communication coefficient between the neighbor agents i and j and N_i is the set of neighbor agents connected to agent i. The information exchange law for the whole system can be written in vector form as

$$X[k+1]=DX[k] \tag{7}$$

where $X[k]$=$[x_1[k],\ldots,x_n[k],\ldots,x_r[k]]^T$ and $X[k+1]$ are the information vector at the k and $k+1$ iteration, respectively, and D is a weight matrix that has the sparsity pattern specified by the communication graph G.

$$D=\begin{bmatrix} 1-\sum\limits_{j\in N_1}a_{1j} & \cdots & a_{1i} & \cdots & a_{1r} \\ \cdots & \cdots & \cdots & \cdots & \cdots \\ a_{i1} & \cdots & 1-\sum\limits_{j\in N_i}a_{ij} & \cdots & a_{ir} \\ \cdots & \cdots & \cdots & \cdots & \cdots \\ a_{r1} & \cdots & a_{ri} & \cdots & 1-\sum\limits_{j\in N_r}a_{rj} \end{bmatrix} \tag{8}$$

If the sums of D's rows and columns are equal to one and the eigenvalues of D satisfy $|\lambda_n|\leq 1$, then we have (9) based on the *Perron–Frobenius Lemma* [21] with $\mathbf{1^T}=\{\mathbf{1},\mathbf{1},...,\mathbf{1}\}^\mathbf{T}$

$$J=\lim_{k\to\infty}D^k=\frac{\mathbf{1}\cdot\mathbf{1}^T}{r} \tag{9}$$

This property of the D matrix implies that the system will reach average consensus (10) as the iteration number k approaches infinity. The average of dispersed network states information ($X[0]$) can be obtained by each agent in a distributed and iterative manner.

$$\lim_{k\to\infty}X[k]=\lim_{k\to\infty}D^kX[0]=\frac{\mathbf{1}\cdot\mathbf{1}^T}{r}X[0] \tag{10}$$

This study adopted the D-matrix by the *Mean Metropolis* method [29] with the following law (11) due to the properties of stability, adaptivity, and faster convergence speed.

$$a_{ij}=\begin{cases} 2/(g_i+g_j+1) & j\in N_i \\ 1-\sum\limits_{j\in N_i}2/(g_i+g_j+1) & i=j \\ 0 & otherwise \end{cases} \tag{11}$$

where g_i and g_j are the number of agents connected to agent i and j, respectively. Since it may take a long time for the average consensus algorithm to achieve the exact equilibrium, it is necessary to define a termination criterion. The required number of iterations for convergence can be approximately determined by (12) when a pre-defined error tolerance (E) is used to reach a consensus [21].

$$K=\frac{\log E}{\log\|D-J\|}=\frac{\log E}{\log\|\lambda_2\|} \tag{12}$$

where $E = \frac{\|X^K - X^\infty\|}{\|X^0 - X^\infty\|}$ is the error tolerance (taken as $1e-6$), and λ_2 is the second-largest eigenvalue of D and the largest eigenvalue of $D - J$, K is the number of iterations for convergence. The derivation process of (12) is given in the appendix B.

In practice, the communication graphs are viewed as time-varying due to the stochastic link failures. For a network of r nodes, there are a total of m possible communication graphs. We denote the set of all possible graphs by $G_1, \ldots, G_m$, and the set of corresponding weight matrices by $D_1, \ldots, D_m$, which is determined by the *Mean Metropolis* method. Then, the iterative distributed information discovery process can be written as

$$X[k+1] = D[i(k)]X[k] \tag{13}$$

where the indices $i(k)$ are integers and satisfy $1 \leq i(k) \leq m$ for all k. The sequence $i(k)_{k=0}^{\infty}$ can be deterministic or stochastic. Then, we have the following convergence theorem for a subset of the graphs that occur infinitely in the sequence. Please see appendix A for the proof of *Theorem 1*.

Theorem 1: *if the collection of communication graphs that occur infinitely often are jointly connected, then the iterative process converges with the Mean Metropolis weights, and*

$$\lim_{k\to\infty} X[k] = \lim_{k\to\infty} (\prod_{k} D[i(k)])X[0] = \frac{\mathbf{1}\cdot\mathbf{1}^T}{r}X[0] \tag{14}$$

This theorem only requires the long-term connectivity of the communication graph. It does not require each link to be active for an infinite amount of time. The only requirement is that the surviving links make a connected graph in the long-term run. In this sense, the distributed average consensus is robust to temporary and permanent link failures.

In our context, the average consensus algorithm is utilized for collecting the state information of ACs that is required for the conventional TPC control, such as the ON/OFF states, indoor temperatures, and electrical powers. To obtain this information, each agent is initialized with an $A_{n\times 3}$ matrix. In matrix A, only the rows corresponding to the agents' number can have nonzero elements. $A(i,1)$ can be equal to either 1 or 0 to represent whether the AC is turned on or off. $A(i,2)$ is equal to its normalized indoor temperature by (15), and $A(i,3)$ is equal to its electrical powers. For example, if the i^{th} AC consumes 5kW, the i^{th} row of its A matrix is initialized with [1 T_i^{norm} 5] and the remaining elements are all equal to zeros.

$$T_i^{norm} = \frac{T_i - T_i^{lower}}{T_i^{upper} - T_i^{lower}} \tag{15}$$

By applying the average consensus law (10) to each initial matrix, all the information matrices will converge to the same matrix. Each element is the average summation of the corresponding elements in the initial matrices. The state information of all ACs in the network can be discovered by reorganizing and rescaling the converged information matrix.

Based on the converged A matrix of each AC, we can divide the ACs into ON/OFF groups by counting the non-zero elements in the first column of the converged matrix. Then the priority lists can be generated for both groups by sorting the elements ascending and descending,respectively, in the second column of the converged matrix. The third column can reveal the ACs' electrical powers by multiplying them by the total number of ACs. The final discovered information is then used for local TPC control, including the ON/OFF temperature priority lists and ACs' electrical powers. For easy explanation, an example with five ACs is presented in Fig. 4.

C. Local temperature priority-based control and trial calculation schemes

Then, each AC can decide its switching actions by executing the conventional TPC method locally based on the local priority lists. The local TPC control is demonstrated in Fig. 5. The x-axis denotes the number of DR-participating AC units, and the double y-axes represents the available flexibility resources (left) and the accumulated power adjustments (right), respectively. The numbers in the square blocks are priority values, and the smaller values represent higher priorities for DR participation. p is the number of ACs in ON/OFF priority lists. The threshold value i for selecting the DR-participating units is determined by the requested DR amount indicated by a dashed line. The red blocks denote the AC units that should be switched for demand response. All DR-participating AC units follow the common rule: *All ACs belonging to the set of red blocks should be switched immediately for demand response*. Here, we assume each AC knows the total number of agents and the required DR amounts of belonging aggregators. Such information could be obtained in a similar distributed way, but they are not discussed here.

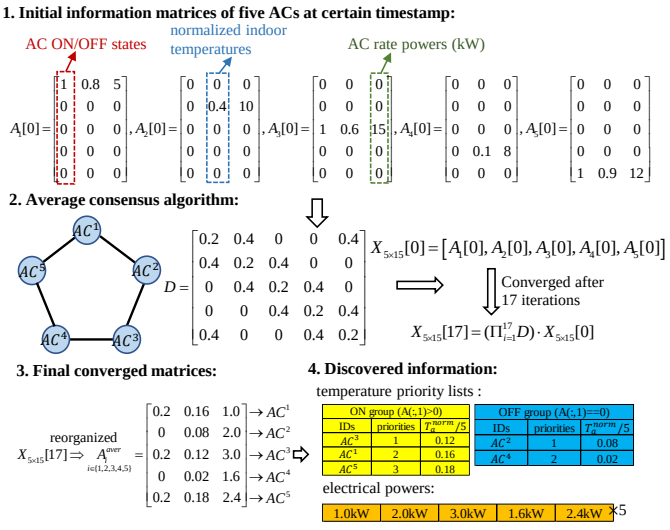

Fig. 4: Illustration of the distributed sensing algorithm for a network of five ACs with ring graph.

Finally, this study proposed trial calculation schemes to 1) filter out unstable control actions that may induce simulation oscillations and users' comfort violations, and 2) calculate the maximum up/downregulation reserve capacity in real-time, as shown in Fig. 6. The trial calculations are implemented twice. In Fig. 6a, the actual control output by a local TPC controller is sent to the house thermal forecaster along with other inputs such as weather data and internal load to predict the indoor temperature of the next timestep. Any controls

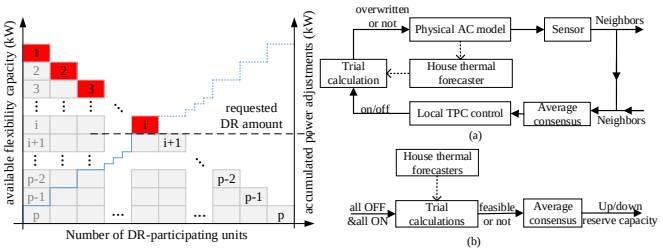

Fig. 5: An illustration of the local TPC controller.

Fig. 6: Trial calculation schemes of ACs.

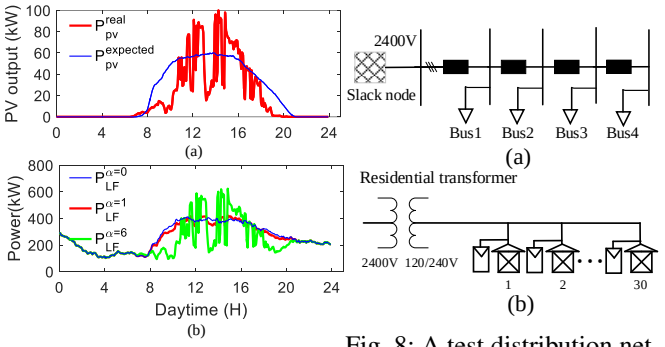

Fig. 7: (a) Deviations between actual and forecasted PV outputs and (b) emulated load following signals (α=0,1,6).

Fig. 8: A test distribution network model with (a) four-bus three-phase feeder and (b) an aggregator at each phase of each load bus.

expected to violate user comfort limits at the next timestep will be overwritten. In Fig. 6b, the virtual 'ALL ON' and 'ALL OFF' controls are sent to house thermal forecasters to check the feasibility and calculate the maximum up/downregulation reserve capacities. The maximum regulation capacity will be uploaded to the upper levels for constraints update (5). Such information could be obtained by the aggregator in a similar distributed way, but they are not discussed here.

IV. SIMULATION SETUPS

Two case studies are simulated for two purposes: 1) validation and analysis of proposed distributed TPC strategy, and 2) application of distributed TPC strategy to smart grid voltage control.

First, one hundred AC units are modeled in MATLAB by ETP models in (2) with heterogeneous parameters and shifted and scaled solar and internal heat gains. Then, they are coordinated by the distributed TPC to respond to load following (LF) signals [14] established by (16).

$$\left.\begin{array}{l}\Delta P_{pv}-\Delta P_L=0\\ \Delta P_{pv}=P_{pv}^{real}-P_{pv}^{\exp ected}\\ \Delta P_L=P_{LF}-P_L^{base}\end{array}\right\}\Rightarrow P_{LF}=P_L^{base}+\alpha\cdot\Delta P_{pv} \quad (16)$$

where ΔP_{pv} is the PV output deviations from the forecasted values, calculated by P_{pv}^{real} minus $P_{pv}^{expected}$, ΔP_L is the load adjustment for system rebalance. P_L^{base} is the expected aggregated load of uncoordinated ACs by using the perfect next-day input forecasts, P_{LF} is the load following signal for real-time system balance. Here, the 'virtual' PV variations ΔP_{pv} are known and are used to emulate the system balancing signals, and α is a coefficient to adjust the degree of PV deviations. Fig. 7 shows the profiles of P_{pv}^{real}, $P_{pv}^{expected}$, and different LF signals with α=0,1,6.

Second, a Gridlab-d/MATLAB co-simulation testbed is established as Fig. 8 to leverage the distributed TPC control strategy for smart grid voltage control. We build a four-bus three-phase electricity distribution feeder in Gridlab-d, an electrical distribution network simulator, to calculate power flows. The feeder is connected with an ideally large grid through the slack bus and consists of four load buses. Each phase at each bus is populated with 30 residential houses equipped with heterogeneous DR-engaged ACs and distributed PV panels. The PVs are sized to induce under-voltage and over-voltage issues in the remote node. Then, the tri-level voltage control framework in Fig. 2 is adopted for voltage regulation.

Without specification, all simulations used ring topology for distributed TPC in this study. All ACs operate in the cooling mode with the same indoor temperature settings of 70 (F) and the same upper and lower temperature limits of 76 (F) and 64 (F). To model the thermal heterogeneity of different buildings, the authors make random samples of the initial indoor temperatures, initial ON/OFF states, and the thermal parameters of each AC model from *Uniform(U)* distributions, as summarized in Table I.

TABLE I: A random sampling of main parameters for the modeling of heterogenous ACs

Parameters	Descriptions	Range	Unit
U_a	Heat transfer coefficient between indoor and outdoor air	$U[400,600]$	$Btu/F.h$
C_a	Heat capacity of the indoor air	$U[600,3000]$	Btu/F
U_m	Heat transfer coefficient between indoor air and building mass	$U[1e4,1.2e4]$	$Btu/F.h$
C_m	Heat capacity of building mass	$U[3250,500]$	Btu/F
μ_{AC}	Coefficient of performance for air conditioners in cooling mode	$U[2.8,3.4]$	–
P_{AC}	Electrical power	$U[5,6]$	kW

V. RESULTS AND DISCUSSIONS

A. Validation and analysis of distributed TPC strategy

In the case of the light LF signals (α=1), it is observed in Fig. 9a that one hundred of ACs can effectively track the load balancing signals. Fig. 9b shows the indoor temperatures always lie between the users' comfort limits during the load following process. The average temperature varies near the value of 70 due to the large temperature diversity of the AC cluster and the insignificant LF signals. It is also observed that the thermal diversities of DR-controlled ACs slightly reduced than that of no DR controls.

However, this is not the case for severe LF signals (i.e., $\alpha = 6$). Fig. 10a shows that the severe LF signals were not well tracked in time intervals of 12:00-13:00, 14:00-15:00, and 18:00-20:00. This is attributed to the clipping of maximum available up/down regulation reserve and the override of control actions by the trial calculation schemes in Fig. 6. As a result, the temperature profiles always lie between the user's thermal comfort limits. Fig. 11 shows the clipping effect of maximum available up/downregulation reserves calculated by

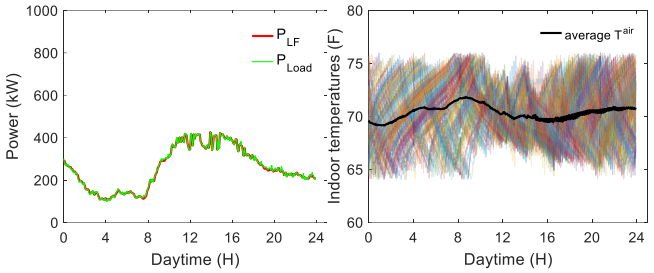

(a) (b)

Fig. 9: System balancing results for the light case (α=1).

the trial calculation scheme. Since the outdoor temperatures are high and most ACs are in 'ON' states to cool indoor air during the daytime, the maximum up-regulation reserve (red curve) is low, and the down-regulation reserve (blue curve) is high. As the degree of PV deviations increases, the issued DR amount (green curve) also increases and hits the reserve limits during noontime.

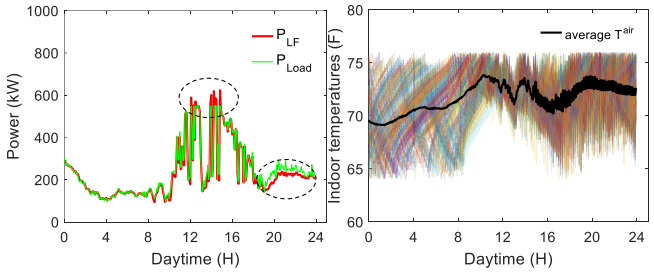

(a) (b)

Fig. 10: System balancing results for the severe case (α=6).

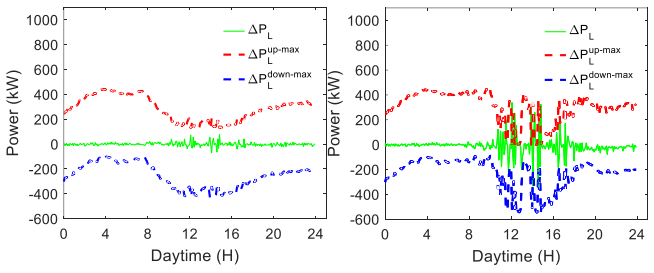

(a) (b)

Fig. 11: Provided load adjustments and the up/down reserve bounds under (a) light DR signal with α=1 and (b) severe DR signal with α=6.

Fig. 12a shows the average indoor temperatures of all ACs under different LF signals (α=0,1,2,3,4,5,6), respectively. They share similar fluctuating patterns with that of the power errors between baseload and different LF signals ($-\Delta P_L = P_L^{base} - P_{LF}$) in Fig. 12b. It validates the effectiveness of distributed TPC for system rebalancing. The average indoor temperatures are always higher than the base scenario—the higher degree of PV variations, the higher the average indoor temperatures. This is because the actual energy consumptions of all ACs are always less than the energy consumptions of the base scenario (see Fig.7b). Fig. 13 shows the statistics of total ACs' switching times under different degrees of LF signals. It is seen that the average switching frequency of ACs increases with the degree of PV forecast errors. However, the increased switching frequency is still acceptable.

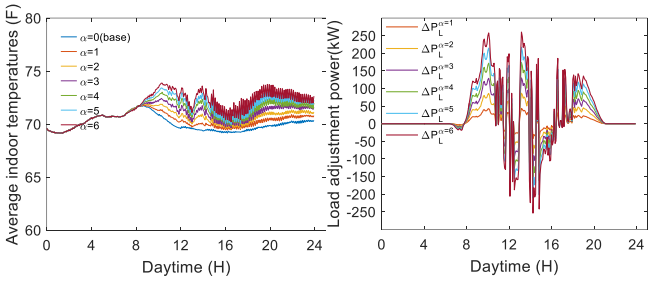

(a) (b)

Fig. 12: System balancing under different LF signals: (a) verage indoor temperatures of 100 ACs, and (b) power errors between base load and LF signals.

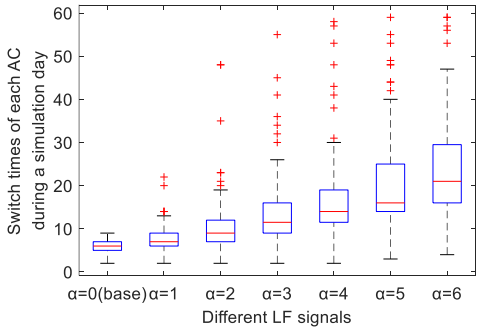

Fig. 13: Statistics of ON/OFF switching times for each AC under different degrees of LF signals.

B. Robustness to communication delays and link failures

If stochastic communication delays are present, the average consensus algorithm can be expressed as

$$x_i[k+1] = x_i[k] + \sum_{j \in N_i} a_{ij}(x_j[k-s] - x_i[k]) \quad \sum_{s=0}^{\tau} f_s = 0, s = 0, 1, ..., \tau \tag{17}$$

where s is the realized time delays following the distribution of f_s, τ is the upper bound of considered time delays. It is proved that a consensus can still be achieved regardless of the presence of the delays, provided that the network has a spanning tree. Nevertheless, the non-zero communication delays will result in deviated consensus value, and the deviations depend on the distribution of s and the dynamics of x.

Fig. 14 demonstrated through a network of five ACs that the distributed TPC with delays has evolutional stability and deviated consensus equilibrium. We assume each AC at each timestep received the lagged information from its neighbors with a probability of 0.2, independent of other nodes and all

previous steps. The number of iteration delays is randomly sampled from a uniform distribution $[1, \tau]$ with an upper bound of $\tau = 5$ iterations. It is observed that the system could achieve convergence very quickly under stochastic communication delays. Nevertheless, the consensus values have apparent deviations from the actual average values (blue lines). Though the consensus deviations of temperatures and powers cause errors to the local priority lists, the delays have no impact on the ON/OFF state estimation of ACs due to the binary output. Thus, one possible way to reduce delay impacts is to transmit all the information through binary codes.

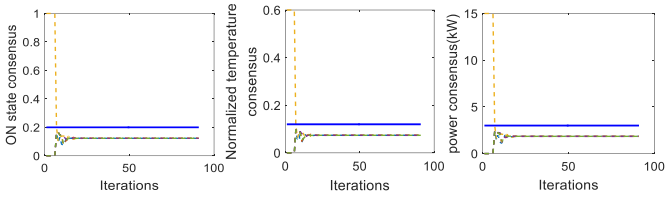

(a) (b) (c)

Fig. 14: Evolutional stability and deviated consensus equilibrium for the AC^3 state information in Fig. 4 when stochastic communication delays are present: (a) ON state consensus; (b) normalized indoor temperature consensus; (c) power consumption consensus.

Fig. 15 compared the ON-group priority lists generated by a consensus network of 50 ACs with and without delays..When there are no communication delays, the red blocks in Fig. 15a represent the ON units that should be switched off to provide down-regulation of 100kW among 50 ACs. Then, we remapped the local TPC results of ON groups without delays to that of considering delays in Fig. 15b. It is observed a large proportion of ACs can still act correctly under stochastic delays. This is because the binary control outputs made the distributed TPC insensitive to the deviated consensus equilibrium.

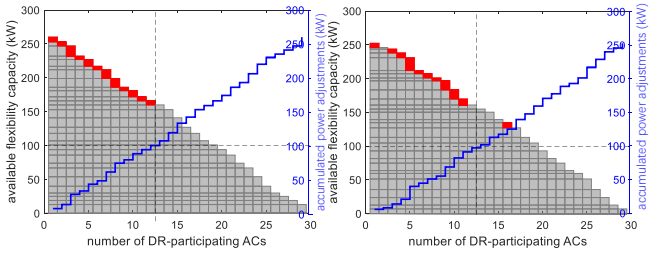

(a) (b)

Fig. 15: Local TPC results for a consensus network of 50 ACs, (a) ON group without delays, and (b) ON group with delays.

As for link failures, we have proved in *Theorem 1* that the distributed average consensus with *Mean Metropolis* weights is robust to temporary and permanent link failures. We demonstrated it by simulating the iterative process with five and fifty ACs, respectively, under static and dynamically changing communication graphs. We assume that each edge in the original

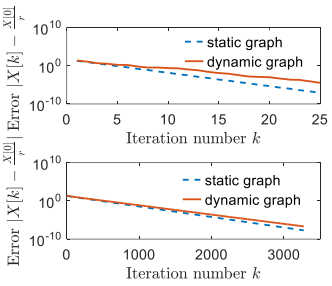

Fig. 16: Norm-1 consensus errors for networks of five and fifty ACs with static and dynamic graphs.

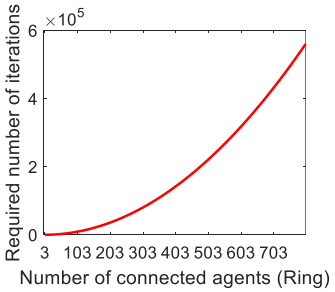

Fig. 17: Iterations for convergence dramatically increase with network sizes for ring graphs.

static graph is not available with a probability of $1/5$ at each timestep independent of other edges and previous steps. The errors between iteratively updated consensus values and the true average values are plotted against the number of iterations in Fig. 16. It is observed that the errors always converge to a nearly-zero value after a certain number of iterations, whether for static or dynamic communication graphs. It is reasonable that the convergence rates with dynamic graphs are slightly slower than that of static graphs, considering the lack of information updates.

C. Scalability to a large number of ACs

We plot the relationship between the required number of iterations and the number of ACs in Fig. 17. It is seen the required number of iterations dramatically increases when the number of agents exceeds 100. It can be explained mathematically. According to (12), the increasing rate of required iteration numbers depends on the changing rate of $|\lambda_2|$. Since we know $|\lambda_1|$ is 1, we can express $|\lambda_2|$ by the spectral gap $\Delta|\lambda|$ (defined as the difference between the moduli of the two largest eigenvalues of the D matrix): $|\lambda_2| = 1 - \Delta|\lambda|$. According to the *Cheeger inequalities* [30], the moduli of the second largest eigenvalue satisfy the following:

$$1 - 2h(G) \leq |\lambda_2| \leq 1 - \frac{h^2(G)}{2\Delta(G)} \tag{18}$$

where $h(G)$ is the *Cheeger constant* of the communication graph and $\Delta(G)$ is the maximum degree of the graphs. For graphs with ring shape topology, the *Cheeger constant* is $h(G) = \frac{2}{\lfloor r/2 \rfloor}$. Then, we plot $|\lambda_2|$ and its upper and lower bounds in Fig. 18. It is observed that the $|\lambda_2|$ (red curve) and its lower bounds (dotted blue curve) quickly approaches one as the network size increases. Thus, the required number of iterations by (12) quickly increases.

We compare the required iteration numbers of one consensus for different communication graphs (i.e., path, ring, rectangular, and cube grid graphs in Fig. 19) with increasing network sizes in Table II. It is seen the required iterations of path and ring graphs quadratically increase with the network sizes. Due to the poor connectivity of the path graph, the required iteration number is quite large, even for small networks (i.e., 8 ACs). In contrast, the graphs with rectangle and cube grid

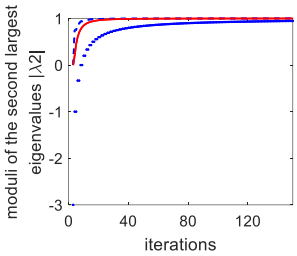

Fig. 18: The moduli of the second largest eigenvalue approach to one quickly with the number of iterations for ring graphs.

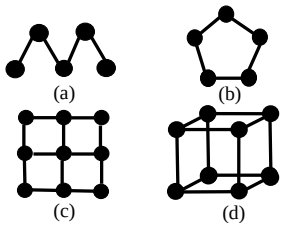

Fig. 19: Examples of communication graphs: (a) path; (b) ring; (c) rectangle grid;(d) cube grid;

topologies have relatively small iteration numbers, increasing linearly with the network sizes. We conclude that the graphs with good connectivity, such as rectangle and cube grid graphs, are scalable to large systems of 4000 ACs, and the ring and path graphs are only applicable to small networks with a few hundred of ACs. Fortunately, the buildings are 3-dimensional cubes, and it is convenient to connect multiple dispersed ACs by 3D grid graphs.

TABLE II: required iteration numbers of one consensus for different graphs with increasing network sizes.

Network sizes		8	64	125	1000	4000
required number of iterations	path	2170	1.4E+4	5.5E+4	3.5E+6	5.6E+7
	ring	52	3580	1.4E+4	8.7E+5	1.4E+7
	rectangle grid	70	372	3531	1.5E+4	4.0E+4
	cube grid	17	116	192	845	3447

D. Voltage regulation performance of proposed control

Fig. 20 and Fig. 21 show the voltage profiles of the fourth load bus in three cases (before DR control, after centralized TPC, after distributed TPC) for under-voltage and over-voltage regulation, respectively. Fig. 20 shows that centralized and distributed control can improve the voltage values to the allowed range during under-voltage periods between 08:00-09:00. In Fig. 21, the voltage regulation performance of distributed TPC is comparable with the centralized one, though there is still a slight over-voltage during 12:30-13:00 by the distributed TPC. It is attributed to the depletion of up-regulation reserve under the proposed trial calculation algorithm.

Fig. 22 plots the time-varying numbers of DR-responding AC units in each bus phase for over-voltage regulation using proposed tri-level voltage control. The positive number of ACs indicates the AC units are being turned on. It is seen the number of DR-responding AC units is always highest in phase A among the three phases. This is due to the more severe voltage violations in phase A. As expected, the total number of DR-responding AC units increases as the target bus moves away from the source bus, validating the necessity of voltage sensitivity-based optimal DR resource dispatch.

VI. Conclusion

This study developed a distributed temperature priority-based ON/OFF control of AC clusters to provide continuous

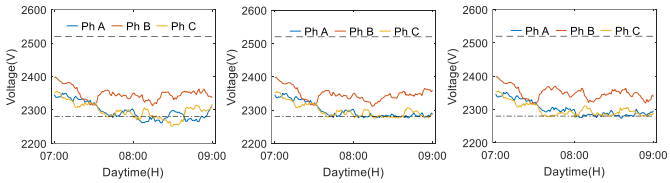

Fig. 20: Under-voltage issue of the fourth load bus (a) before DR control, (b) after centralized TPC, (c) after distributed TPC

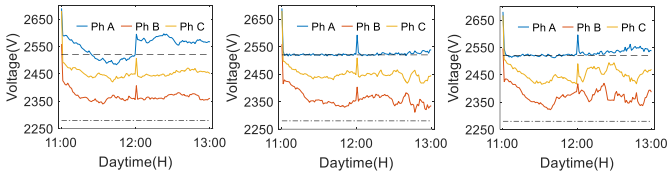

Fig. 21: Over-voltage issue of the fourth load bus (a) before DR control, (b) after centralized TPC, (c) after distributed TPC

system balancing reserves for the smart grid. A novel and practical hierarchical control framework is also proposed for efficient and effective smart grid voltage regulation through strategic selection and permutation of demand response technologies. Numerical simulations validated the effectiveness of distributed TPC and the tri-level hierarchical control framework for system rebalancing and voltage regulation under high PV penetrations.

Through theoretical and numerical analysis, we proved that the distributed TPC scheme with *Mean Metropolis* weights is stable under time-varying communication graphs with stochastic link failures and insensitive to the communication delays due to the ON/OFF binary control outputs. We found that the average consensus algorithm is not scalable to large systems for graphs with bad connectivities (i.e., path, ring shapes). The required number of iterations for convergence dramatically increases after the number of agents exceeds a threshold value. In contrast, graphs with good connectivity (i.e., rectangle and cube grid graphs) could increase the network size to 4000 ACs with an acceptable number of necessary iterations. Future extensions may include the experimental design and test of proposed algorithms in both laboratory and practice scenarios and the development of delay-tolerant consensus algorithms for accurate distributed sensing.

Appendix A
Proof of Theorem 1

The *Theorem 1* has been proved [31] for average consensus algorithms with *Uniform* and *Metropolis* weights. Both *Uniform* and *Metropolis* weight matrices are doubly stochastic matrices. However, the D matrix with *Mean Metropolis* weights is not doubly stochastic because the diagonal elements may become negative. Thus, the authors proved here that the *Theorem 1* is applicable for average consensus algorithm with

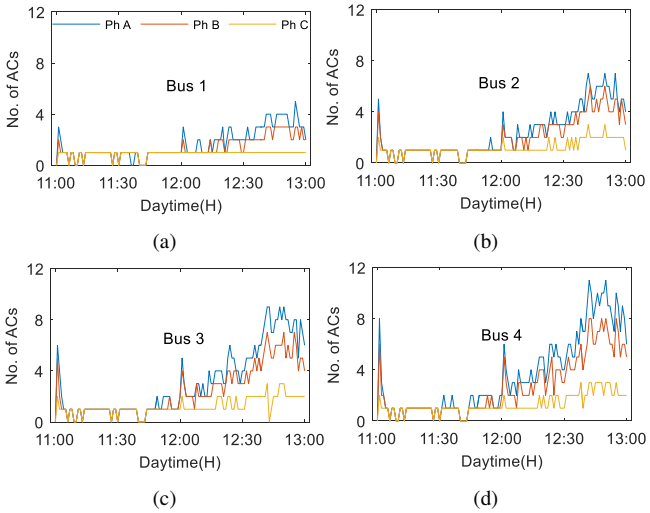

Fig. 22: Numbers of DR-participating ACs at each phase of each bus for over-voltage regulation using distributed TPC

Mean Metropolis weights. The proof of *Theorem 1* is based on a convergence result of nonhomogeneous infinite products of paracontracting matrices in *Theorem 2* (Please see reference [32], [33] for details).

Theorem 2: *Suppose that a finite set of square matrices* $\{D_1, \ldots, D_m\}$ *are paracontracting. Let* $i(k)_{k=0}^{\infty}, 1 \leq i(k) \leq m$*, be a sequence of integers, and denote* I *the set of all integers that appear infinitely in the sequence. Then for all* $X[0] \in R^n$ *the sequence of vectors* $X[k+1] = D[i(k)]X[k], k \geq 0$*, has a limit of* $X^{\infty} \in \bigcap_{i \in M} H(D[i])$ *where* $H(D)$ *denote the fixed-point subspace of a paracontracting matrix* D*, i.e., its eigenspace associated with the eigenvalue 1,* $H(D) = \{x \,|\, x \in R^n, Dx = x\}$ To use the result of *Theorem 2*, we need to use the following two lemmas.

Lemmas 1: For any graph, the matrix D with *Mean Metropolis* weights is paracontracting with respect to the Euclidean norm.

Lemmas 2: If a collection of graphs $G_1, \ldots, G_m$ are jointly connected, their corresponding *Mean Metropolis* weight matrices satisfy $\bigcap_i^m H(D[i]) = span\{\mathbf{1}\}$.

According to Lin [31], when D matrix satisfies the above two Lemmas, the *Theorem 1* can be proved. Thus, in the following, the authors proved that the two lemmas apply to the *Mean Metropolis* matrix.

Proof of lemma 1: According to the concept of paracontracting matrices, a symmetric matrix is paracontracting with respect to the Euclidean norm if and only if all its eigenvalues lie in the interval $(-1, 1]$. Since the D matrix is apparently a symmetric matrix, there is no complex eigenvalues and we only need to prove the eigenvalues of D matrix lie in the interval $(-1, 1]$. The D weight matrix can write as $D = E - A$, where E is the identity matrix, and A can write as

$$A = \begin{bmatrix} \sum\limits_{j \in N_1} a_{1j} & \cdots & -a_{1i} & \cdots & -a_{1r} \\ \cdots & \cdots & \cdots & \cdots & \cdots \\ -a_{i1} & \cdots & \sum\limits_{j \in N_i} a_{ij} & \cdots & -a_{ir} \\ \cdots & \cdots & \cdots & \cdots & \cdots \\ -a_{r1} & \cdots & -a_{ri} & \cdots & \sum\limits_{j \in N_r} a_{rj} \end{bmatrix} \tag{19}$$

Let μ,λ be the eigenvalues of D and A matrices, we have μ=1-λ. Since that the absolute values of non-diagonal elements all lie in $[0, 1)$, all eigenvalues of A are in the disks $|\lambda - \Delta| \leq \Delta$,with $\Delta = \sum_{j \in N_i} a_{ij}, i \in \{1, ..., r\}$, according to the *Gershgorin disk theorem*. As the eigenvalues of a real symmetric matrix are real, we have $\lambda \geq 0$.

Let v be an eigenvector of the eigenvalue λ of A matrix, and v_k is the element of v with largest absolute value ($|v_k| \geq |v_i|, i \in \{1, \ldots, r\}, i \neq k$). Then

$$\begin{aligned} &Av = \lambda v \Rightarrow \sum_j A_{kj} v_j = \lambda v_k \\ &|\lambda v_k| = |\lambda|\,|v_k| = \left|\sum_j A_{ij} v_j\right| \leq \sum_j |A_{ij}|\,|v_k| \leq (\sum_j |A_{ij}|)\,|v_k| \\ &\Rightarrow |\lambda| \leq \sum_j |A_{ij}| \Rightarrow \lambda \leq \sum_j |A_{ij}| \end{aligned} \tag{20}$$

Let n be the number of connected agents for i^{th} node in the consensus graph, so there are n non-zero non-diagonal elements of i^{th} row of A matrix and the degree of i^{th} node is $g_i = n$. Then, we have

$$\begin{aligned} &|A_{ij}| = \tfrac{2}{g_i + g_j + 1} = \tfrac{2}{n + g_j + 1} \leq \tfrac{2}{n+2} \Rightarrow \sum_j |A_{ij}| \leq \tfrac{2n}{n+2} < 2 \\ &\lambda \leq \sum_j |A_{ij}| < 2 \end{aligned} \tag{21}$$

The feasible zone of D's eigenvalues is determined as

$$\lambda \in [0, 2), \mu = 1 - \lambda \Rightarrow \mu \in (-1, 1] \tag{22}$$

Therefore, the matrix D with *Mean Metropolis* weights is paracontracting with respect to the Euclidean norm.

Proof of lemma 2: By definition (11), the sum of rows of *Mean Metropolis* weight matrices always equal to one, so we have $\mathbf{1}$=$[1, \ldots, 1]^T \in H(D[i])$ for $i = 1, \ldots, m$. Therefore,

$$span\{\mathbf{1}\} \subset \bigcap_i^m H(D[i]) \tag{23}$$

Since $D[i]x = x$ for $i = 1, \ldots, m$, then we have $\left(\frac{1}{m}\sum_{i=1}^m D[i]\right) x = x$. Therefore

$$\bigcap_i^m H(D[i]) \subset H(\frac{1}{m}\sum\nolimits_{i=1}^m D[i]) \tag{24}$$

Since the collection of graphs $G_1, \ldots, G_m$ are jointly connected, the matrix $\frac{1}{m}\sum_{i=1}^m D[i]$ has a trivial eigenvector $\mathbf{1}$ associated with an eigenvalue 1. Next, we show $\mathbf{1}$ is the only eigenvector associated with the eigenvalue of 1. Since $E - D$ is a weighted Laplacian matrix and the collection of graphs are jointly connected, the matrix $E - D$ has the rank of $n - 1$. Let x be any eigenvector associated with the eigenvalue 1, the null space of $\lambda x - Dx = (E - D)x = 0$ only has one basis vector. Thus, $\mathbf{1}$ is the only eigenvector of $\frac{1}{m}\sum_{i=1}^m D[i]$ associated with the eigenvalue of 1. Therefore,

$$H\left(\frac{1}{m}\sum\nolimits_{i=1}^m D[i]\right) = span\{\mathbf{1}\} \tag{25}$$

Putting the equations (23)-(25) together, we get the *Lemma 2* result.

APPENDIX B
DERIVATION OF EQUATION (12)

Given the properties of D matrix: $D\mathbf{1} = \mathbf{1}, \mathbf{1}^T D = \mathbf{1}^T$ and the projection matrix [34]: $I - \frac{\mathbf{1}\mathbf{1}^T}{r} = \left(I - \frac{\mathbf{1}\mathbf{1}^T}{r}\right)^K$, we have:

$$\begin{aligned} &D^K - J = (D - J)^K \\ &(D^K - J) \cdot X^{\infty} = 0 \end{aligned} \tag{26}$$

The error at iteration K is defined as:

$$\begin{aligned}&\left\|X^K - X^\infty\right\| = \left\|(D^K - J)X^0\right\| \\ &= \left\|(D^K - J)(X^0 - X^\infty)\right\| \leq \|D - J\|^K \left\|X^0 - X^\infty\right\|\end{aligned} \tag{27}$$

Let define the error tolerance $E = \frac{\left\|X^K - X^\infty\right\|}{\|X^0 - X^\infty\|}$, the required number of iterations can be obtained as

$$K = \frac{\log E}{\log \|(D - J)\|} \tag{28}$$

According to the Gelfand's formula: $\rho(D - J) = \lim_{k\to\infty} \left\|(D - J)^k\right\|^{\frac{1}{k}} = |\lambda_{max}|$, we can express the required number of iterations in terms of the spectral radius of $D - J$ matrix:

$$K = \frac{\log E}{\log |\lambda_{max}|} \tag{29}$$

where λ_{max} is the largest eigenvalue of $D - J$ matrix.

Let arrange the n eigenvalues of D as 1, λ_2, ..., λ_n, with the decrease of their magnitudes. 1 is the largest eigenvalue of D and $\mathbf{1}$ is the corresponding eigenvector. Since the eigenvectors of a symmetrical matrix are orthogonal, i.e.$\mathbf{1^T e_j = 0}$ for $j \geq 1$ where e_j is the corresponding eigenvector of λ_j, we have $(D-J)e_j = De_j - \frac{\mathbf{1}\mathbf{1}^T}{r}e_j = De_j = \lambda_j e_j$. Since $(D-J)\mathbf{1} = D\mathbf{1} - \frac{\mathbf{1}\mathbf{1}^T}{r}\mathbf{1} = 0$, the eigenvalues of $D - J$ are λ_2, ..., λ_n,0 with the decrease of their magnitudes. Now λ_2 becomes the eigenvalue of $D - J$ with the largest magnitude. We have

$$K = \frac{\log E}{\log |\lambda_2|} \tag{30}$$

REFERENCE

[1] C. Gonzalez, J. Geuns, S. Weckx, *et al.*, "Lv distribution network feeders in belgium and power quality issues due to increasing pv penetration levels," in *2012 3rd IEEE PES Innovative Smart Grid Technologies Europe (ISGT Europe)*, IEEE, 2012, pp. 1–8.

[2] F. M. Uriarte, A. Toliyat, A. Kwasinski, and R. E. Hebner, "Consumer-data approach to assess the effect of residential grid-tied photovoltaic systems and electric vehicles on distribution transformers," in *2014 IEEE 5th International Symposium on Power Electronics for Distributed Generation Systems (PEDG)*, IEEE, 2014, pp. 1–8.

[3] E. Demirok, P. C. Gonzalez, K. H. Frederiksen, D. Sera, P. Rodriguez, and R. Teodorescu, "Local reactive power control methods for overvoltage prevention of distributed solar inverters in low-voltage grids," *IEEE Journal of Photovoltaics*, vol. 1, no. 2, pp. 174–182, 2011.

[4] H. Bevrani, B. François, and T. Ise, *Microgrid dynamics and control*. John Wiley & Sons, 2017. DOI: 10.1002/9781119263739.

[5] M. Zeraati, M. E. H. Golshan, and J. M. Guerrero, "Distributed control of battery energy storage systems for voltage regulation in distribution networks with high pv penetration," *IEEE Transactions on Smart Grid*, vol. 9, no. 4, pp. 3582–3593, 2016.

[6] L. Y. Seng and P. Taylor, "Innovative application of demand side management to power systems," in *First International Conference on Industrial and Information Systems*, IEEE, 2006, pp. 185–189.

[7] Q. Xie, H. Hui, Y. Ding, *et al.*, "Use of demand response for voltage regulation in power distribution systems with flexible resources," *IET Generation, Transmission & Distribution*, vol. 14, no. 5, pp. 883–892, 2020.

[8] E. L. Ratnam and S. R. Weller, "Receding horizon optimization-based approaches to managing supply voltages and power flows in a distribution grid with battery storage co-located with solar pv," *Applied Energy*, vol. 210, pp. 1017–1026, 2018.

[9] Z. Jiang, J. Cai, and P. S. Moses, "Smoothing control of solar photovoltaic generation using building thermal loads," *Applied Energy*, vol. 277, p. 115 523, 2020.

[10] C. V. Chandran, M. Basu, K. Sunderland, S. Pukhrem, and J. P. Catalão, "Application of demand response to improve voltage regulation with high dg penetration," *Electric Power Systems Research*, vol. 189, p. 106 722, 2020.

[11] H. Fontenot, K. S. Ayyagari, B. Dong, N. Gatsis, and A. Taha, "Buildings-to-distribution-network integration for coordinated voltage regulation and building energy management via distributed resource flexibility," *Sustainable Cities and Society*, vol. 69, p. 102 832, 2021.

[12] A. Klem, M. H. Nehrir, and K. Dehghanpour, "Frequency stabilization of an islanded microgrid using droop control and demand response," in *2016 North American Power Symposium (NAPS)*, IEEE, 2016, pp. 1–6.

[13] T. Jiang, Z. Li, X. Jin, H. Chen, X. Li, and Y. Mu, "Flexible operation of active distribution network using integrated smart buildings with heating, ventilation and air-conditioning systems," *Applied energy*, vol. 226, pp. 181–196, 2018.

[14] N. Lu and Y. Zhang, "Design considerations of a centralized load controller using thermostatically controlled appliances for continuous regulation reserves," *IEEE Transactions on Smart Grid*, vol. 4, no. 2, pp. 914–921, 2012.

[15] X. Wu, J. He, Y. Xu, J. Lu, N. Lu, and X. Wang, "Hierarchical control of residential hvac units for primary frequency regulation," *IEEE Transactions on Smart Grid*, vol. 9, no. 4, pp. 3844–3856, 2017.

[16] X. Hu and J. Nutaro, "A priority-based control strategy and performance bound for aggregated hvac-based load shaping," *IEEE Transactions on Smart Grid*, vol. 11, no. 5, pp. 4133–4143, 2020.

[17] C. Winstead, M. Bhandari, J. Nutaro, and T. Kuruganti, "Peak load reduction and load shaping in hvac and refrigeration systems in commercial buildings by using a novel lightweight dynamic priority-based control strategy," *Applied Energy*, vol. 277, p. 115 543, 2020.

[18] R. Olfati-Saber, J. A. Fax, and R. M. Murray, "Consensus and cooperation in networked multi-agent systems," *Proceedings of the IEEE*, vol. 95, no. 1, pp. 215–233, 2007.

[19] J. Khazaei and Z. Miao, "Consensus control for energy storage systems," *IEEE Transactions on Smart Grid*, vol. 9, no. 4, pp. 3009–3017, 2016.

[20] Y. Du, H. Tu, H. Yu, and S. Lukic, "Accurate consensus-based distributed averaging with variable time delay in support of distributed secondary control algorithms," *IEEE Transactions on Smart Grid*, vol. 11, no. 4, pp. 2918–2928, 2020.

[21] M. Zeraati, M. E. H. Golshan, and J. M. Guerrero, "A consensus-based cooperative control of pev battery and pv active power curtailment for voltage regulation in distribution networks," *IEEE Transactions on Smart Grid*, vol. 10, no. 1, pp. 670–680, 2017.

[22] M. Zeraati, M. H. Golshan, and J. M. Guerrero, "Voltage quality improvement in low voltage distribution networks using reactive power capability of single-phase pv inverters," *IEEE transactions on smart grid*, vol. 10, no. 5, pp. 5057–5065, 2018.

[23] B. Wang, T. Zhang, X. Hu, Y. Bao, and H. Su, "Consensus control strategy of an inverter air conditioning group for renewable energy integration based on the demand response," *IET Renewable Power Generation*, vol. 12, no. 14, pp. 1633–1639, 2018.

[24] C. Chen, J. Wang, and S. Kishore, "A distributed direct load control approach for large-scale residential demand response," *IEEE Transactions on Power Systems*, vol. 29, no. 5, pp. 2219–2228, 2014.

[25] F. M. Atay, "Consensus in networks under transmission delays and the normalized laplacian," *IFAC Proceedings Volumes*, vol. 43, no. 2, pp. 277–282, 2010.

[26] D. Wang, C. S. Lai, X. Li, *et al.*, "Smart coordination of virtual energy storage systems for distribution network management," *International Journal of Electrical Power & Energy Systems*, vol. 129, p. 106 816, 2021.

[27] L. Tesfatsion and S. Battula, "Notes on the gridlab-d household equivalent thermal parameter model," 2020.

[28] S. Weckx, R. D'Hulst, and J. Driesen, "Voltage sensitivity analysis of a laboratory distribution grid with incomplete data," *IEEE Transactions on Smart Grid*, vol. 6, no. 3, pp. 1271–1280, 2014.

[29] Y. Xu and W. Liu, "Novel multiagent based load restoration algorithm for microgrids," *IEEE Transactions on Smart Grid*, vol. 2, no. 1, pp. 152–161, 2011.

[30] J. Cheeger, "A lower bound for the smallest eigenvalue of the laplacian," *Problems in analysis*, vol. 625, no. 195-199, p. 110, 1970.

[31] L. Xiao, S. Boyd, and S. Lall, "A scheme for robust distributed sensor fusion based on average consensus," in *IPSN 2005. Fourth International Symposium on Information Processing in Sensor Networks, 2005.*, IEEE, 2005, pp. 63–70.

[32] D. J. Hartfiel, *Nonhomogeneous matrix products*. World Scientific, 2002.

[33] L. Elsner, I. Koltracht, and M. Neumann, "On the convergence of asynchronous paracontractions with application to tomographic recon-

struction from incomplete data," *Linear Algebra and its Applications*, vol. 130, pp. 65–82, 1990.

[34] L. Xiao and S. Boyd, "Fast linear iterations for distributed averaging," *Systems & Control Letters*, vol. 53, no. 1, pp. 65–78, 2004.

Zhuang Zheng (Member, IEEE) received the B.E. degree in Electrical Engineering and Automation from Zhejiang University, China, in 2017, and the Ph.D. degree in Architecture and Civil Engineering from City University of Hong Kong, Hong Kong SAR, in 2021. He is currently a Postdoctoral Research Fellow with the Department of Built Environment and Energy Engineering, The Hong Kong Polytechnic University. His research interests include smart energy management in power grid and built environment, grid-interactive and energy-flexiable buildings, optimal design and operation of low-carbon building/district energy systems.

Shengwei Wang received the BEng and MSc degrees in Refrigeration and Air-conditioning from Huazhong University of Science and Technology (HUST) in 1983 and 1986, respectively, and his Ph.D. degree in HVAC and Building Automation from the University of Liege in 1993. He is currently a chair professor and the director of the Research Institute for Smart Energy with The Hong Kong Polytechnic University. His research expertise and interests cover energy systems and building automation systems, energy-flexible buildings and demand response in smart grid, zero/low energy buildings, smart and distributed energy systems, cleanroom air-conditioning systems, district and data center cooling systems, uncertainty analysis in building and system design and control/diagnosis, next-generation key technologies for smart buildings.

Wenzhuo Li received a B.Sc. degree in Building Environment and Equipment Engineering from Nanjing University of Science and Technology, Nanjing, China, in 2015, and an M.Eng. degree in Heating, Gas Supply, Ventilating, and Air Conditioning Engineering from Harbin Institute of Technology, Harbin, China in 2017, and the Ph.D. degree from the Department of Building Services Engineering, Hong Kong Polytechnic University, Hong Kong, China in 2021. Her research interests include distributed optimization for optimal control of heating, ventilation, and air conditioning systems and Internet of Things (IoT) technologies in smart building automation systems. She is currently a Postdoctoral Research Fellow with the Bartlett School of Environment, Energy and Resources, University College London, London, UK.

Xiaowei Luo received a B.Sc. degree in the Department of Civil Engineering from Tsinghua University in Beijing, China, in 2003, an M.S degree in Construction Management from Tsinghua University in 2006, and the Ph.D. degree in Construction Engineering and Project Management from the University of Texas at Austin in 2013. He is currently an Associate Professor in the Department of Architecture and Civil Engineering at the City University of Hong Kong. His main research interests include Building Information Modeling, Construction Safety Management, Information Technology in Construction, Wireless Sensor Technologies, and Green Building. His current research projects focus on the development and deployment of information and sensing technologies to advance construction safety and efficiency as well as improve the quality and sustainability of construction projects.